Spatial differences in wind-driven sediment resuspension in a shallow, coastal estuary

Anthony C. Whipple[a,*], Richard A. Luettich Jr.[a], Janelle V. Reynolds-Fleming[b], Ryan H. Neve[a]

[a] University of North Carolina Institute of Marine Sciences, 3431 Arendell St., Morehead City, NC 28512, USA
[b] Seahorse Coastal Consulting, LLC, 3103 Mandy Lane, Morehead City, NC 28557, USA

ARTICLE INFO

Keywords:
Estuary
Sediment
Resuspension
Turbidity
USA
North Carolina
New river
Autonomous vertical profiler

ABSTRACT

Two locations approximately 11 km apart along the axis of the New River Estuary near Jacksonville, NC USA were continuously monitored for eight years. Included in the observations are vertical profiles of turbidity, temperature, salinity, chl-a, dissolved oxygen, pH and water velocity as well as local wind velocity. Differences between the two sites result from a number of factors, including bathymetry, wind strength, direction and fetch, estuarine morphology, tidal currents and sediment properties. The site near the head of the estuary, Morgan Bay, is deeper, experiences generally weaker winds and has less fetch in most directions. Stones Bay, the down-estuary site, is shallower, experiences stronger winds and has longer fetch, particularly in the prevailing wind directions. Current speeds also differ along the estuary with the down-estuary Stones Bay site being more tidal.

The observations were used together with a simple wave model to analyze the estuarine turbidity response to different forcing mechanisms. Results suggest that sediments are resuspended primarily by wind-wave generated bottom stress at both locations. While turbidity is generally higher in Stones Bay than in Morgan Bay, turbidity as a function of the local wave-induced bottom stress (including forcing from all directions) is similar at both locations at low stress but diverges at higher stresses. At higher bottom stresses, turbidity in Stones Bay responds primarily to winds from the NE, S and NW while turbidity in Morgan Bay responds primarily to winds from the NW and S. Accounting for sediment resuspension within an approximate spatial advection scale around each of the observation sites, yields a similar turbidity vs bottom stress response curve for the three primary directions in Stones Bay and the S direction in Morgan Bay but a greater turbidity response for winds from the NW in Morgan Bay. In the latter case, waves are crossing the section of the New River Estuary just downstream of the confluence with the New River and are presumably encountering sediments that are more easily resuspended.

Average sediment export is down-river with more sediment leaving Stones Bay than Morgan Bay.

1. Introduction

Understanding sediment dynamics is critical to understanding the morphology of estuaries (Dalrymple et al., 1992) and to understanding many of the physical, chemical, and biological processes taking place within them (e.g. Dyer, 1989). Resuspension of a thin layer of sediment can release enough nutrients to more than double the overlying productivity (Fanning et al., 1981; Fisher et al., 1982). Resuspended sediment can also carry with it viable populations of meiofauna (Bell and Sherman, 1980) and algae such as benthic diatoms (Schallenberg and Burns, 2004, De Jonge and van Beusekom, 1995) as well as viral and bacterial material (Fries et al., 2006) that have been buried or were residing in the bed. Spatial and temporal variability of resuspension can create similar variability in biological responses in the system (Hall et al., 2013).

Resuspension can be caused by a variety of physical processes, including tidal and wind-driven currents and wind waves. Resuspension by tidal currents has been observed in many estuaries (c.f. Bell and Sherman, 1980; Hamblin, 1989; Sanford et al., 1991) and can be the primary cause of suspended sediment in strongly tidal systems. Wind waves have been observed to resuspend bottom sediments in shallow environments where waves interact with the sea floor (Ward et al., 1984; Lavelle et al., 1978) and in many cases have been deemed the most important input to the sediment resuspension process (Lesht et al., 1980; Clark et al., 1982; Luettich et al., 1990; Sanford, 1994; Schoellhamer, 1995; Nakagawa et al., 2000).

Recent studies have applied complex coupled models to predict suspended sediment concentrations in semi-enclosed or coastal water

* Corresponding author.
E-mail address: whipple@email.unc.edu (A.C. Whipple).

https://doi.org/10.1016/j.ecss.2018.08.005
Received 1 March 2016; Received in revised form 2 August 2018; Accepted 10 August 2018
Available online 11 August 2018

bodies. Lee et al. (2007) used a 3D circulation model based on the Princeton Ocean Model, a parametric two-dimensional surface wind wave model, and a depth-averaged, two-dimensional mixed sediment transport model (SEDGL2D) to model the suspended sediment plume in southern Lake Michigan noting that both wave conditions and sediment bed properties are critical factors in determining resuspension and the suspended sediment distribution. Liu and Huang (2009) considered wind-induced sediment transport in Apalachicola Bay, FL, using the 3D Environmental Fluid Dynamics Code (EFDC) model and a coupled 3D sediment transport model. Computed suspended sediment concentrations for two storm events were 10 times background concentrations and compared with field observations. No explicit attribution was made of the role of waves vs currents. Ji and Jin (2014) used EFDC coupled to the SWAN wave model to demonstrate that wave induced stress was an essential driver of sediment dynamics in Lake Okeechobee, FL. In a series of papers, Carniello et al. (2011, 2012, 2014) modeled sediment dynamics in Venice Lagoon using a wind-wave tidal model (WWTM) coupled with a sediment transport and bed evolution module (STABEM). The authors identified multiple processes affecting suspended sediment concentrations, including: erosion by wind waves on tidal flats and by tidal currents in deeper tidal channels; the sheltering effect of intertidal landforms; the importance of accounting for both cohesive and noncohesive sediments; and the stabilizing effect of benthic vegetation on sediment resuspension. Bever and MacWilliams (2013) used a coupled 3D hydrodynamic, wave and sediment model (including four sediment size classes) to reproduce suspended sediment concentration in San Francisco Bay. They identified the importance of including wind waves to properly capture erosion on shoals. Bever et al. (2018) found that an observed decrease in wind speed over the past two decades translated to a decrease in turbidity up to 55 percent in parts of San Francisco Bay. Escobar and Velasquez-Montoya (2017) modeled seasonal patterns of suspended sediment concentration in the Gulf of Urabá, Columbia using Delft3D coupled with SWAN and a 3D sediment transport model for cohesive and noncohesive sediments. Similar to the other studies, they found waves effects on suspended sediment concentration are enhanced in shallow waters. Only a few studies have identified the influence of wind direction on suspended sediment in semi-enclosed waterbodies. Bever et al. (2018) noted that stormy years had more variation in dominant wind direction than less stormy years in San Francisco Bay and that this should have implications for turbidity in fetch limited estuaries. Further work on the influence of wind direction on turbidity was recommended. Seers and Shears (2015) found that turbidity in New Zealand's tidal creeks responded more strongly to winds blowing in an offshore direction while turbidity in coastal areas responded more strongly to winds blowing onshore. Wang et al. (2018) analyzed satellite imagery to conclude that wind direction impacted both resuspension and advection of turbidity from Hangzhou Bay into the East China Sea.

These studies document progress over the past several decades in understanding and predicting field scale suspended sediment dynamics. In many cases they reflect improvements in observational technology (e.g., in situ sensors, satellite imagery and improved methods for processing this imagery) and modeling (e.g., the development of coupled hydrodynamic and sediment transport models). Virtually all conclude that wind waves are key drivers of resuspension in shallow water depths, although there is considerable diversity in the assumptions and parameters (e.g., size classes, erosion rates, critical stresses, flocculation, settling rates, space and time variability of parameters) that are used to model resuspension and suspended sediment concentrations. Most studies have worked with high temporal resolution field data that were collected over limited durations (e.g., weeks to months), longer time series (e.g., years) that were sampled less frequently (e.g., monthly), or high spatial resolution data (satellite imagery) that is available infrequently in time.

Our study takes advantage of a novel data set comprised of turbidity and wind velocity data with high temporal resolution (half hourly) spanning an extended time period (eight years) from two field sites 11 km apart in the shallow, nearly enclosed, New River Estuary near Jacksonville, NC, (Fig. 1). We also have much shorter water velocity records (5 months) that are sufficient to characterize tidal currents at each location. Thus, we are able to resolve from super-tidal to inter-annual turbidity responses at these two closely located sites and the local forcing that contributed to these responses over a wide range of time scales and meteorological conditions, ranging from a few hours to substantial storm events. Given the small size of the estuary, the large amount of data and the wide range of conditions, we pursued a simplified, mechanistic approach to relating the turbidity response at our field sites to the local forcing. This approach provided substantial insight into the turbidity response without requiring the specification of multiple model parameters, most of which are still poorly known in this and similar estuarine systems.

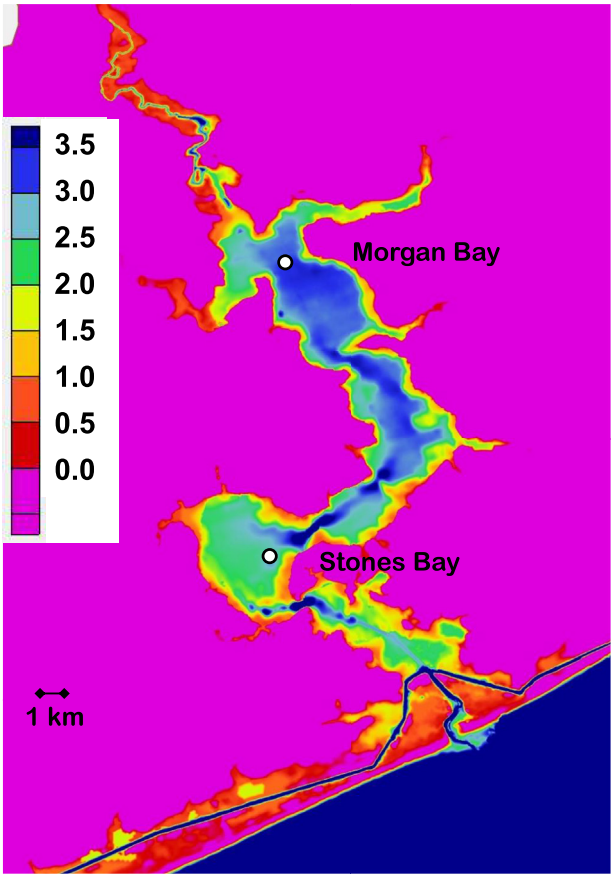

Fig. 1. Bathymetry of the New River Estuary near Jacksonville, North Carolina USA. Depths are shown in meters. The marked locations are sites of both autonomous vertical profiler (AVP) and acoustic Doppler current profiler (ADCP) data collection.

Beginning in the early 1940s much of the New River Estuary has been part of the Marine Corps Base Camp Lejeune, one of the largest marine training facilities on the east coast. Since 2005, water quality within the estuary has been monitored with a particular focus on excess nutrient loading. Resuspension of sediments and the mechanisms that cause resuspension are of interest in order to better understand the nutrient cycle in the estuary, the overall water quality and other ecosystem processes.

2. Methods

2.1. Setting

The New River Estuary is connected to the open ocean through a

narrow inlet that restricts exchange. The drainage basin of the New River Estuary is fairly small at approximately 1400 km^2. Freshwater input is episodic and ranges from a few m^3s^{-1} in the absence of local rainfall, to 100–250 m^3s^{-1} during and immediately after heavy rains. Two sites were chosen in the estuary, one in the upper estuary in Morgan Bay and one in the lower estuary in Stones Bay (Fig. 1). The Morgan Bay site is approximately 3.5 m deep and is somewhat sheltered from the wind with typical fetch lengths of 1–3 km. The Stones Bay location is slightly shallower and more exposed with average water depths of 2.5 m and fetch lengths of 2–4 km. The combined semi-diurnal and diurnal tidal amplitudes are 10 cm and 17 cm in Stones Bay and Morgan Bay whereas total water level may vary by as much as 80 cm at each site. Grain size analyses of surface grab samples taken at each site show that Morgan Bay sediments have a unimodal distribution with a peak size of 53 μm, and that 99% of the distribution is less than 130 μm. Stones Bay has a bi-modal distribution with peaks at 14 and 95 μm. The minimum between the peaks lies at the 37th percentile, and 99% of the distribution is less than 180 μm.

2.2. Autonomous Vertical Profilers

From June 2008–October 2016 Autonomous Vertical Profilers (AVPs) were deployed at each of the two sites in the New River Estuary. The AVPs have evolved over the years from the design published in Reynolds-Fleming et al. (2002). The current AVPs are equipped with YSI 6600 sondes and are configured to produce a water column profile of temperature, salinity, turbidity, pH, dissolved oxygen and chlorophyll fluorescence every half hour. The instruments are programmed to sample once per second and data is collected during the descent from surface to bottom at a velocity of approximately 4 cm s^{-1}. Sondes are exchanged with freshly calibrated ones monthly or sooner if necessary due to excessive drift in the data, malfunction, or bio-fouling. Anemometers (RM Young Marine Wind Monitor 0510) mounted approximately 4 m above the water line measure 6 min averages of wind speed and direction every 30 min. Wind velocities were averaged over 2 h intervals for the analyses presented herein. Data are stored on-board and telemetered nightly for processing. Both AVPs remained operational from 2008 to 2016 with only brief interruptions yielding a nearly continuous eight-year dataset that is comprised of approximately 140,000 vertical profiles at each location.

AVP profile data are post-processed in several steps before they are ready for analysis. These steps include filtering, outlier elimination, visual inspection, and post-calibration sensor correction. The on-board filtering in the YSI 6600 sondes is turned off during data collection to eliminate any vertical shift in the data caused by the time lag in the filter response while the sonde is moving. The optical sensor data for turbidity and chlorophyll fluorescence are smoothed in post-processing with a bi-directionally applied second order Butterworth low pass filter with a 10 s period. Data from the other sensors are left unfiltered. Next, data are checked for outlier values. All data are then subjectively checked visually. This allows elimination of data for reasons that would be difficult to detect objectively such as profiler malfunctions and bio-fouling. Post calibration corrections are then applied to the data based on the following: 1) when the sondes are exchanged, the old (previously deployed) sonde and the new (about to be deployed) sonde are placed side-by-side in a sample of water and simultaneous observations are made; 2) AVP profiles from the old and new sondes taken adjacent in time are compared; and 3) during post-processing, values are compared across the entire time series to help detect if a newly deployed sonde had problems with its laboratory calibration. Lastly, the vertically averaged turbidity is obtained from each profile for the analyses described below.

2.3. ADCP deployments

A 1200 kHz Teledyne RDI Acoustic Doppler Current Profiler (ADCP) was deployed near each AVP for a 5-month period from mid-July to mid-December 2009. Since the New River estuary is a fairly shallow water environment, the ADCPs were mounted nearly flush with the estuary floor. This was done by designing mounting hardware for the ADCPs that allowed them to be held in the interior of a length of twelve-inch diameter schedule 40 PVC pipe. During deployment the PVC pipe was driven into the sediment and enough sediment was removed from the interior to mount the ADCP in place. Adjusting the ADCP's default blanking distance parameter allowed the first bin of ADCP data to be collected at 0.5 m above bottom. The instrument was programmed in fast ping-rate mode 12 using 20 pings per ensemble and collected profiles in 10 cm bins every 6 min. This configuration of the ADCP yields an internal variability in velocity measurement with a standard deviation of 1.27 cm s^{-1}.

2.4. Waves

We did not have instrumentation to directly measure wind waves. To estimate wave conditions near the AVPs, a simple wave model, the Wave Exposure Model (WEMo) developed by the National Oceanic and Atmospheric Administration was used (Malhotra and Fonseca, 2007). WEMo is based on scaling laws for fetch- and depth-limited waves, which are well established for locally generated wind waves (e.g. USCOE, 1977; Luettich and Harleman, 1990), and also accounts for shoaling, bottom friction and breaking. While not previously applied to the New River Estuary, WEMo has been validated in a nearby coastal estuary of similar physical dimensions (Malhotra and Fonseca, 2007). Bathymetry and shoreline data for the entire New River Estuary and wind speed and direction were given as inputs to the model. Wave parameters were calculated for each AVP location and other points throughout Morgan and Stones Bays (section 4), based on a series of 56 evenly spaced wind directions and wind speeds ranging from 1 to 20 m s^{-1}. Outputs include the wave height, wave period, orbital velocity, shear stress, and shear velocity. These parameters were then arranged in the form of a lookup table indexed by wind speed and direction. Wave conditions for observed winds were calculated by interpolating linearly between values in the lookup table. Due to the small, highly elongated inlet connecting the New River Estuary to the coastal ocean, it was assumed that all waves inside the estuary were locally generated wind waves and not the result of oceanic wind waves or swell.

3. Results

Wind conditions throughout the data collection period are summarized in Fig. 2. The wind rose plots (Fig. 2 a,b) show that winds were most frequently observed blowing from the southwest and northeast which are known to be the seasonally dominant directions in this area for summer and winter respectively. Stones Bay shows both a higher frequency of, and stronger, southwest winds (Fig. 2b). Wind roses for winds in excess of 9 m s^{-1} (Fig. 2 c,d), indicate in Stones Bay these stronger winds occur most frequently from the southwest, although the strongest winds blow from the north and northwest (Fig. 2d). The most frequent direction for strong wind in Morgan Bay is from the northwest, although a significant fraction also comes from the south (Fig. 2c). A hodograph, (Fig. 2e), shows the diurnal wind pattern and helps to clarify the difference in the average winds between the two sites. At both sites, winds from hours 1–10 (representing time-of-day in local standard time) come from the northwest. After this time, the wind in each bay rotates toward the southwest. Stones Bay reaches a stable southwest direction by hour 14 and remains there until hour 17 after which the speed decreases and then begins to veer back to the northwest. Morgan Bay does not stabilize in the southwest direction, but rather continues to rotate throughout the day reaching the southwest direction around hour 14, nearly due south by hour 17 and thereafter rotating back to the northwest. This is consistent with a daily sea breeze

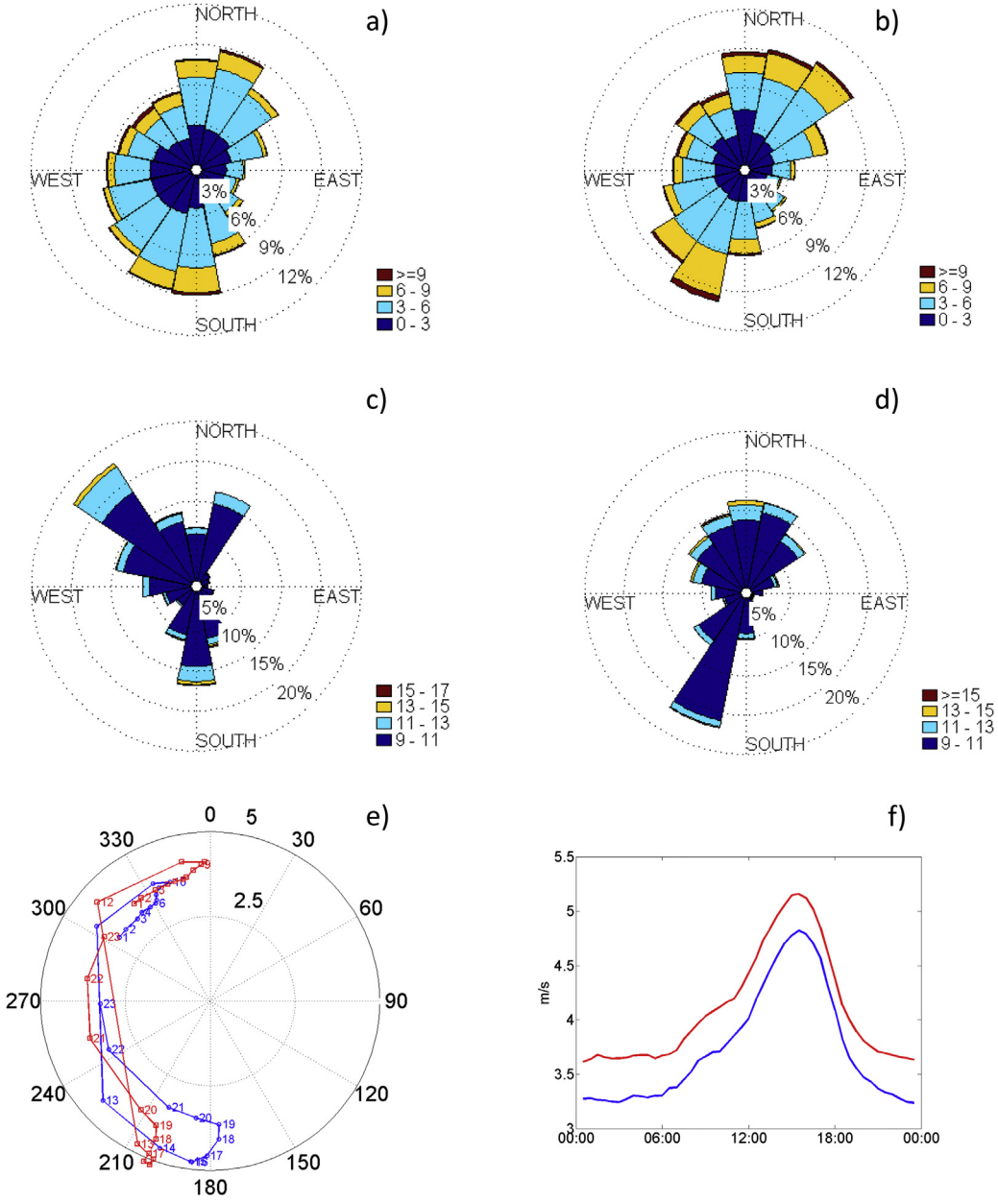

Fig. 2. Wind roses from Morgan Bay (a,c) and Stones Bay (b,d). Directions in the wind roses represent the direction the wind is blowing from. Concentric rings represent the frequency of occurrence. Colors represent different wind speed ranges and radial lengths show the frequency of occurrence of each wind speed range in that direction. Wind roses for all data are presented in a,b. Wind roses for wind speeds greater than or equal to 9 m s^{-1} are presented in c,d. Mean wind hodographs are presented in e; data labels indicate hour of day. Mean wind speeds by time-of-day are presented in f. For e and f, Morgan Bay is in blue and Stones Bay is in red.

that arrives earlier and is more persistent in Stones Bay. The mean wind speed in Stones Bay is about a half meter per second faster than in Morgan Bay (4.1 vs. 3.6 m s^{-1}) and afternoon wind speeds average 1.5 m s^{-1} faster than night/early morning in both locations (Fig. 2f).

Power spectra of the eight years of depth-averaged turbidity data (computed using 63 overlapping, 90-day segments) were computed for each location, (Fig. 3). The majority of the power at both Stones Bay and Morgan Bay is in the low frequency range, presumably associated with meteorological forcing, although significant responses occur in Stones Bay at major astronomical tidal frequencies (O1, K1, M2, S2) and shallow water derivatives (M4, MK3, 2MK3). Turbidity in Morgan Bay does not respond as strongly beyond the low frequency range, although there is a significant response at diurnal and M2 frequencies. Spectral analyses of the wind data (not shown) indicate peaks at 24 h and 12 h, and therefore the turbidity responses at the corresponding frequencies are due to a combination of the astronomical tide and wind. The largest response (Stones Bay at 1 cycle per day) is equivalent to a daily turbidity signal having an amplitude of approximately 1 NTU. As shown below, this is quite small compared to the turbidity change associated with significant resuspension events.

Fig. 4 shows turbidity plotted as a function of several potential forcing variables. In all plots the data were sorted by the x-axis variable value then smoothed by a 100 point moving average filter to reduce variability and expose trends. In order to keep extreme values, the filter length was reduced at either end as necessary to use all available data. Turbidity increases exponentially as a function of wind speed and at the same wind speed, Stones Bay responds with higher turbidity values than Morgan Bay (Fig. 4 a).

During the 5 months of ADCP data, turbidity showed a weak correlation to the total current speed, both in Morgan Bay and in Stones

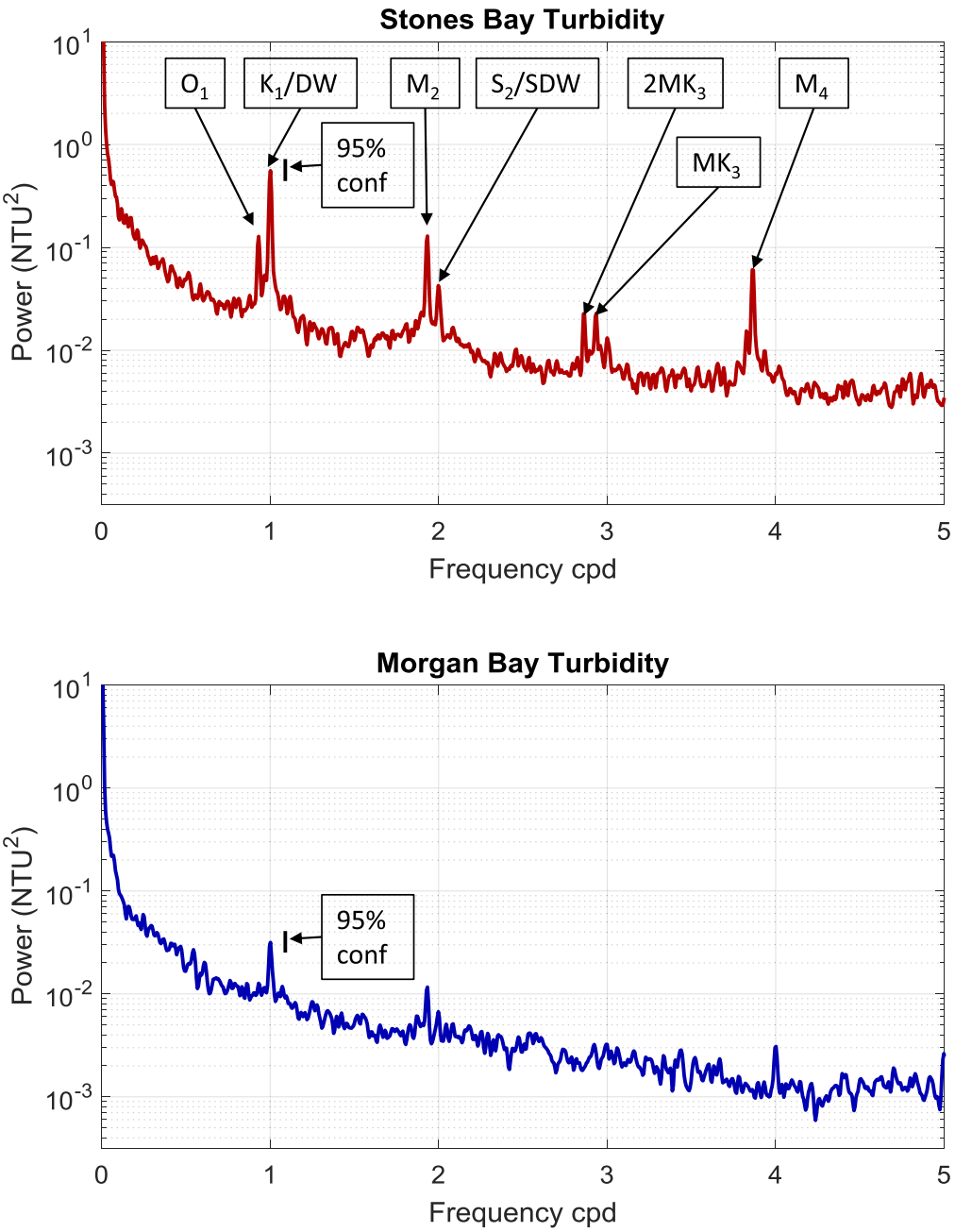

Fig. 3. Power spectra of depth averaged turbidity for Stones Bay (top panel) and Morgan Bay (bottom panel). Tidal constituents are labeled in the top panel with DW representing diurnal wind and SDW representing semi-diurnal wind.

Bay, (Fig. 4b). Harmonic analysis of the ADCP data indicated that astronomical tides account for about 60 percent of the current variability in Stones Bay but only 15 percent in Morgan Bay. Bottom stresses estimated from the mean current fall below 0.05 N m^{-2} which are small compared to the wave stresses (below). Thus the small turbidity responses identified at diurnal frequencies and higher in the power spectral analysis (Fig. 3) are more likely to represent advection of background turbidity than resuspension by currents of corresponding frequencies. Given the strong turbidity response to the wave conditions (below), the weak response of turbidity to the total current speed probably reflects correlation between current speed and wave conditions and not direct current forcing.

Wave heights and bed shear stresses computed from the WEMo wave model for the entire 8 year record of AVP data are also plotted against turbidity (Fig. 4 c,d). The wave conditions computed at the AVP locations take account of the wind speed and the wind direction (via the fetch length and the water depth profile in the upwind direction). Similar to the plots with wind speed, an increasing relationship exists between turbidity and the computed wave height with greater turbidity in Stones Bay than in Morgan Bay for the same wave height, (Fig. 4c). Using wave-induced bottom stress as the forcing variable brings the Morgan Bay and Stones Bay turbidity responses into close alignment below 17 NTUs; above this, turbidity in Stones Bay increases with respect to Morgan Bay, (Fig. 4d).

Significant turbidity events, e.g., turbidity values greater than 10 NTU, corresponded to computed bottom stresses of approximately 0.05 N m^{-2} or greater (Fig. 4e), and occurred rather infrequently during the eight years of data collection. At Stones Bay and Morgan Bay, less than 1 percent and 0.25 percent of the profiles occurred during periods when the computed bottom stress exceeded 0.05 N m^{-2} and

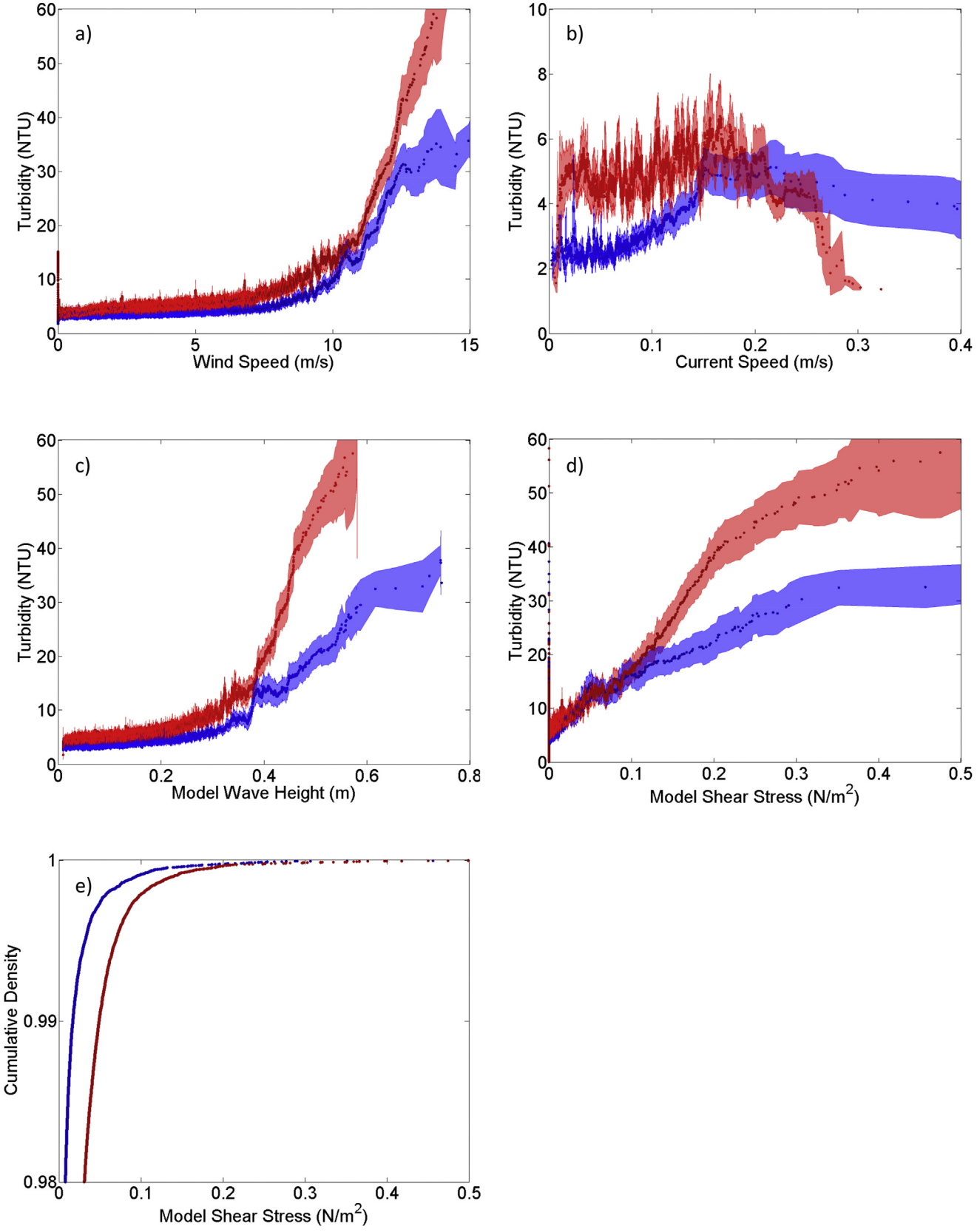

Fig. 4. Turbidity (NTU) as a function of (a) wind speed; (b) current speed from a 5 month subset of the bottom-most bin of the ADCP; (c) WEMo computed wave heights; (d) WEMo computed bed shear stress; and (e) the cumulative density curve for the top 2% of computed bottom stress values. Morgan Bay is in blue and Stones Bay in red. Shaded areas represent 95% confidence intervals. Data in (a)–(d) are smoothed along the x-axis using a 100 point moving average filter with decreasing length at the end of the record.

Table 1
AVP profiles collected during high stress events.

	Total# profiles	# profiles (% of profiles) with bottom stress greater than			
		0.05 Nm^{-2}	0.1 Nm^{-2}	0.2 Nm^{-2}	0.3 Nm^{-2}
Morgan Bay	139,914	337 (0.24%)	114 (0.08%)	31 (0.02%)	8 (0.006%)
Stones Bay	138,628	1201 (0.87%)	226 (0.16%)	45 (0.03%)	19 (0.01%)

less than 0.2 percent and 0.1 percent of the profiles occurred during periods when the bottom stress exceeded 0.1 $N\,m^{-2}$ (Fig. 4e, Table 1). The deployment of the AVP over an extended observation period provided a unique opportunity to capture these significant but relatively rare turbidity events within the New River Estuary.

The relationship between wave stress and turbidity in Stones Bay and Morgan Bay can be further evaluated by considering the turbidity response as functions of both wave stress and wind (wave) direction, (Fig. 5 a,b). A turbidity response greater than 10 NTUs is limited to two wind directions in Morgan Bay (approximately 310–330 deg and 150–170 deg) and three wind directions (approximately 290–310 deg, 190–210 deg and 40–60 deg) in Stones Bay. These correspond closely with the directions of the strongest winds, (Fig. 2 c,d), and for discussion purposes are referred to as NW, S and NE winds, respectively. Separating the turbidity responses into the principal wind directions yields additional perspective on the turbidity vs wave stress relationship. In particular, the two dominant wind directions (NW, S) in Morgan Bay have significantly different turbidity responses, (Fig. 5c), while the turbidity responses in the three dominant wind directions (NW, S, NE) are in relatively close agreement in Stones Bay, (Fig. 5d). Thus the average turbidity response, (Fig. 4d), is representative of the directional response in Stones Bay but not in Morgan Bay.

At the event scale the turbidity response in Stones Bay and Morgan Bay often differed during the same event, (Fig. 6). A NE wind yields low wave stresses at the Morgan Bay site and a relatively low turbidity response (< 10 NTU) that may be due to advection, (Fig. 6a). For example the first pulse of turbidity in the early afternoon of the 24th is coincident with lower salinity water, suggesting an upstream source, while the larger pulse during the morning of the 25th occurs during rising salinity and suggests a downstream source. Wave stresses during the same period at the Stones Bay site were an order of magnitude larger and the turbidity response was substantially greater (> 30 NTU), Fig. 6b. The response at Stones Bay is more closely correlated with the wave stress, although it appears to be modulated by advection at both diurnal and semi-dirunal frequencies, i.e., pulses of lower salinity water indicating down estuary flow seem to also bring lower turbidity water.

Conversely, a S wind event creates greater wave stress at the Morgan Bay site than the Stones Bay site. In this case the Morgan Bay turbidity response was well correlated to the local wave stress (Fig. 6c), while Stones Bay may be responding to advection of turbidity up estuary on the rising tide (Fig. 6d).

Overall, at both sites strong wave stresses (e.g., > 0.05 $N\,m^{-2}$) quickly result in elevated turbidity levels (> 10 NTU) that are presumably of nearby origin; advection modulates this response somewhat

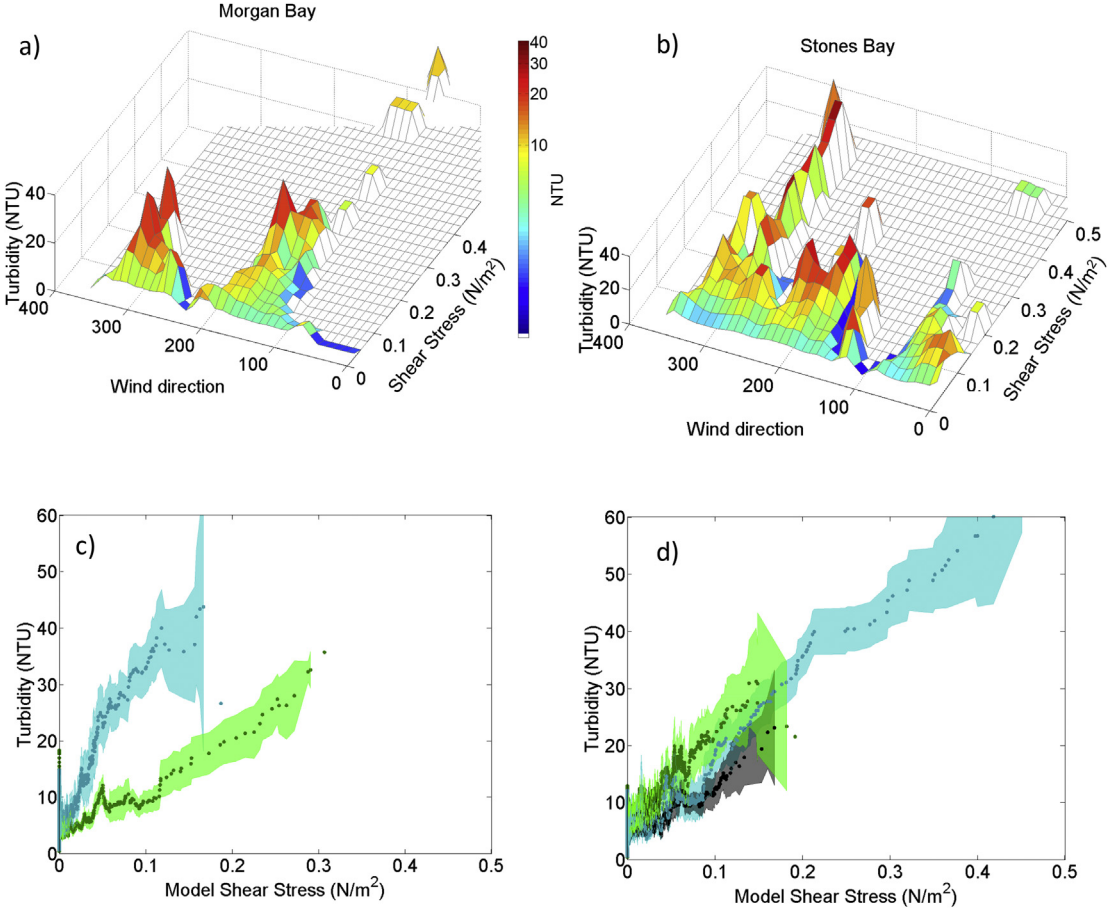

Fig. 5. Turbidity as a function of wind direction and bottom shear stress in (a) Morgan Bay and (b) Stones Bay. Turbidity as a function of bottom shear stress for the principal wind directions in (c) Morgan Bay and (d) Stones Bay. Green represents S winds; cyan represents NW winds; black represents NE winds. Shaded areas represent 95% confidence intervals. Data in (c) and (d) are smoothed along the x-axis using a 30 point moving average filter with decreasing length at the end of the record.

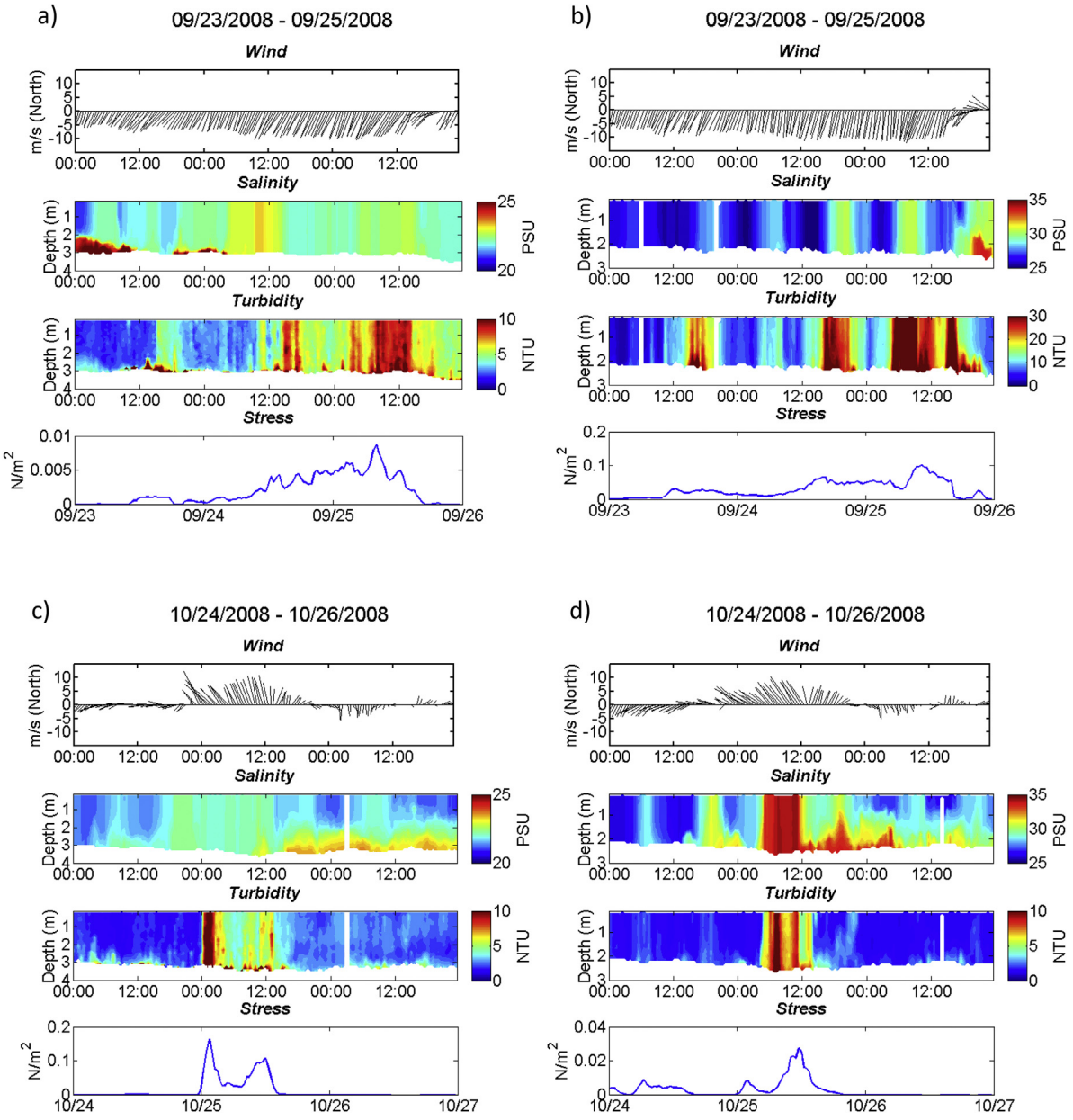

Fig. 6. Wind vectors, profiles of salinity and turbidity, and bottom stress from the AVP site for two, three-day periods of time. Wind vectors point in the direction toward which the wind is blowing. The left column is for Morgan Bay and the right column is for Stones Bay. Note that the salinity range in Morgan Bay is 5 and in Stones Bay it is 10. The turbidity range in (b) has been increased to 30 NTU and the stress scales vary.

and plays a more significant role in turbidity levels at weaker wave stresses.

4. Discussion

As reviewed in the introduction, local wave-induced bottom stress has been shown to provide a reasonable forcing variable for suspended sediment concentrations in many shallow water bodies. In these previous studies wave properties were typically observed (vs modeled in the present study), the measure of turbidity was limited to a single height in the water column (vs full water column profiles in the present study), and temporally dense observations lasted for a few days to weeks (vs 8 years, 140,000 profiles spanning a broad range of meterological forcing in the present study). Wave models have been used in other studies (Carper and Bachman, 1984; Nakagawa et al., 2000; Booth et al., 2000) to calculate bottom stress. The WEMo wave model is based on theory that is well-established for modeling simple wind waves (i.e., in local equilibrium) in fetch- and depth-limited water bodies and it has been successfully validated in a similar shallow enclosed basin to the NRE. Thus we believe it provides a reasonable tool for computing wave properties for our study.

The fetch in Stones Bay is longer in most directions than in Morgan Bay; Stones Bay is about 1 m shallower than Morgan Bay. With longer fetch and shallower water, wind waves should interact more strongly with the bottom and suspend more sediment. This is consistent with our observations that Stones Bay has higher turbidity than Morgan Bay for similar wind speed and computed wave heights (Fig. 4a, c). When turbidity is related to the local wave-induced bottom stress, the directionally aggregated responses in Stones Bay and Morgan Bay are similar, although the turbidity level appears to be limited in Morgan Bay vs Stones Bay at higher stresses (Fig. 4d).

The large size of our data set allowed us to isolate the turbidity response as a function of the dominant wind direction. While the responses in Stones Bay were similar for the three dominant wind

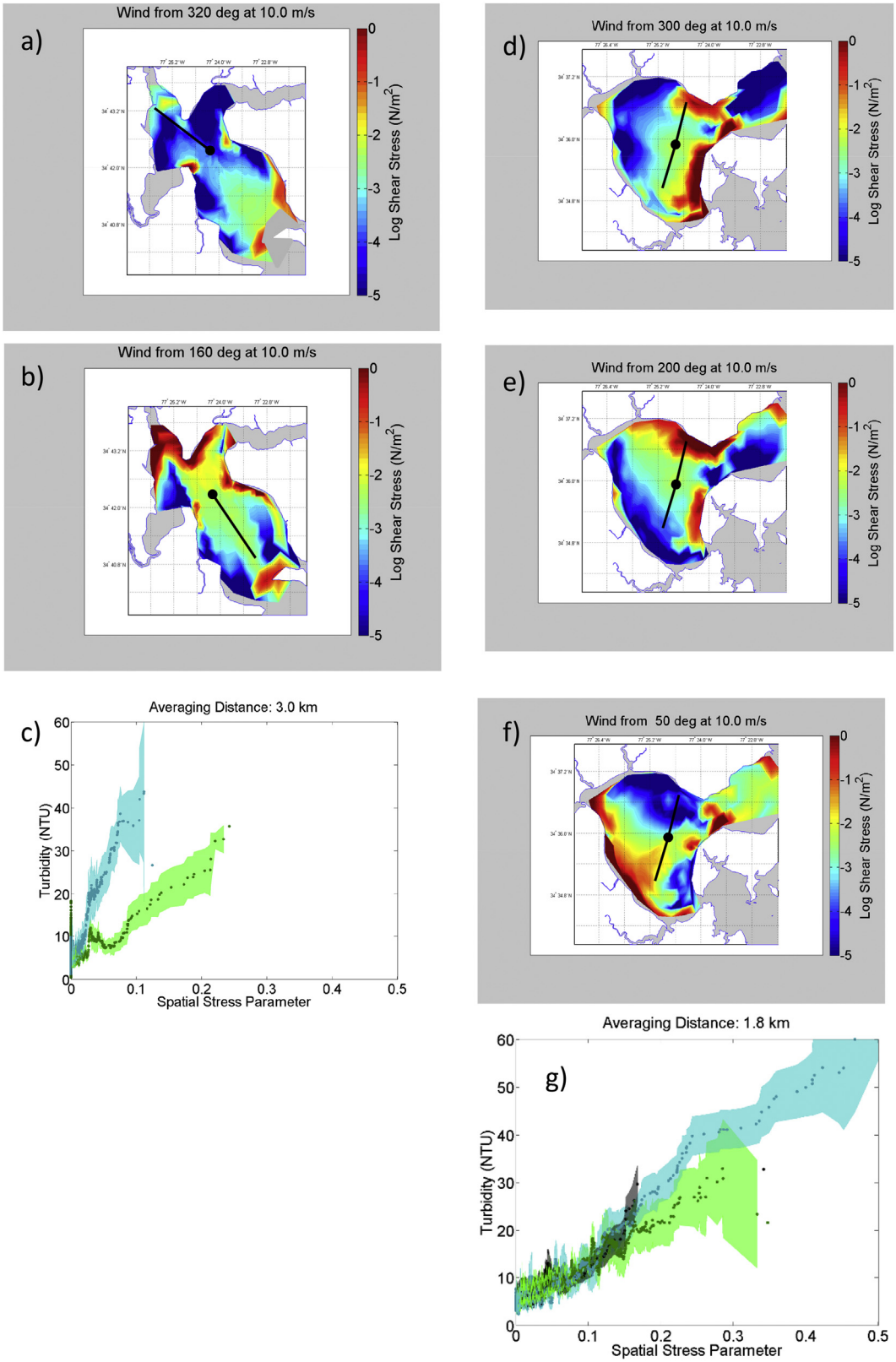

Fig. 7. Spatial distribution of bottom stress for a 10 m s^{-1} wind (a) Morgan Bay from 320 deg, (b) Morgan Bay from 160 deg, (d) Stones Bay from 300 deg, (e) Stones Bay from 200 deg, (f) Stones Bay from 50 deg. Black line segments are drawn from the AVP location 3 km toward the wind in Morgan Bay and 1.8 km in the flood and ebb directions in Stones Bay. Turbidity plotted as a function of the spatial stress parameter in (c) Morgan Bay and (g) Stones Bay. Green represents S winds; cyan represents NW winds; black represents (NE) winds. Shaded areas represent 95% confidence intervals.

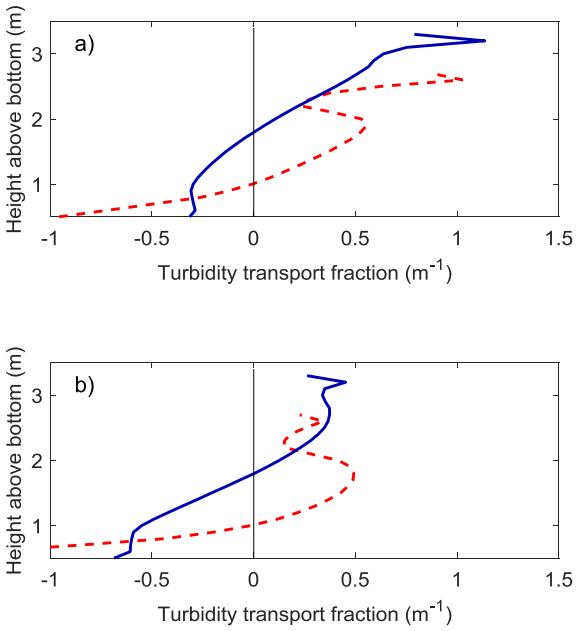

Fig. 8. Profiles of turbidity transport fraction for (a) a uniform distribution of sediment size, (b) a linear distribution of sediment size classes (see text). Morgan Bay is blue (solid) and Stones Bay is red (dashed). Positive values represent downstream transport. (For interpretation of the references to colour in this figure legend, the reader is referred to the Web version of this article.)

directions, Morgan Bay has two distinctly different wave stress versus turbidity relationships. The directionally aggregated response in Morgan Bay is an average of these two directionally dependent responses and thus substantially obscures the actual behavior of the system.

Hamilton and Mitchell (1996) used spatially averaged bottom stress values over an entire basin in a shallow lake to improve predictions of suspended solids concentrations. Given the relatively small size and varying depth in the New River Estuary, and recognizing that advection partially modulates the turbidity response, we examined whether turbidity levels at our sampling sites may reflect resuspension over a spatial area as opposed to being limited to the measurement location and whether this may help explain observed differences in the directional response. Spatial maps of the wave-induced bottom stress were created for the dominant wind directions in both Morgan Bay and Stones Bay. An example for a $10\,m\,s^{-1}$ wind speed indicates a significant variation in stress throughout each bay with highest values located in shallow areas at greatest wind fetch and smallest values located in areas that are deeper or have a small fetch, (Fig. 7 a, b, d, e, f).

We computed average wave-induced bottom stresses over a variety of spatial scales and distributions and used these in place of the local wave-induced bottom stress in Fig. 5. In our case, bay-wide bottom stress averages did not reduce the spread in the directional response in either Stones Bay or Morgan Bay, which is consistent with the relatively short response time between elevated turbidity and significant wave stresses noted previously. However, in Stones Bay, an average wave-induced bottom stress computed over a 1.8 km length (approximately equal to the M2 tidal excursion in that area) aligned with the semi-diurnal tidal current direction (see orientation of black line in Fig. 7 d,e,f) was able to further reconcile the stress vs turbidity response for the three primary wind response directions (Fig. 7 g). Some improvement in the less tidal Morgan Bay (Fig. 7c) was obtained by averaging the wave-induced bottom stress over a distance of 3 km in the upwind direction (see black line in Fig. 7 a,b), although the improvement is marginal and distinct responses remain in the two dominant wind directions.

The results from Stones Bay (Fig. 7g) strongly suggest that turbidity at this location is well represented over a wide range of wind events by an average response over the tidal excursion and that the sediment resuspension rate is approximately homogeneous over this area. The slight divergence of the directional response at the highest stresses may reflect differences in sediment resuspension deeper in the sediment bed, advection from areas with different sediment characteristics or simply the small sample size at the highest bottom stress.

While spatial averaging in the upwind direction did account for some of the directional response in Morgan Bay, the remaining disagreement suggests that other factors, such as sediment characteristics, are important for determining the directional response here. Winds from the NW would resuspend sediment from the area where the New River enters the New River Estuary. It is likely that these sediments are fine, loosely compacted and therefore relatively easy to resuspend compared to sediments further down estuary. Thus it is not surprising that winds from the NW generate greater turbidity than those from the S at this location. A final observation is that the turbidity response corresponding to the S wind at Morgan Bay (green curve in Fig. 7c) is in close agreement with the response in Stones Bay (Fig. 7g), suggesting similarity in the sediment resuspension in Stones Bay and the southern part of Morgan Bay.

Some insight may be gained into the sediment transport characteristics of the New River Estuary by an examination of transport of turbidity. Assuming a linear relationship between NTU and concentration (e.g., Liu and Huang, 2009), which is representative if the sediment properties such as size and shape remain uniform over the range of turbidity values (Conner and De Visser, 1992), the fraction of the total turbidity exported versus imported at the observation site should reasonably represent the fraction of sediment exported versus imported. Profiles of turbidity transport during the period in which the ADCPs were deployed are presented in Fig. 8a. These are calculated as the average of the product of each turbidity profile multiplied by its corresponding along stream velocity profile and then normalized such that the integral of the absolute value equals one. Estuarine flow in both bays cause a net export in the downstream-flowing surface water and a net import in the upstream-flowing bottom water. Stones Bay shows 75% of the total flowing downstream and 25% flowing upstream. Morgan Bay shows 70% flowing downstream and 30% flowing upstream. The river discharge during the duration of the current meter deployment was about 25% greater than the long-term mean.

Since the relationship between sediment concentration and turbidity depends on particle size, we also considered the possibility that sediment size may not have been uniformly distributed through the water column. The above calculations were repeated assuming that particle sizes measured from the bottom grab samples were distributed throughout the water column with the largest particles at the bottom and the smallest at the surface. A linear distribution was used which ranged from the 90th percentile at the bottom to the 10th percentile at the surface. Assuming optical backscatter intensity is inversely proportional to particle diameter (Downing, 2006; Conner and De Visser, 1992) transport was re-calculated, Fig. 8b. Under this scenario, the transport in Morgan Bay changes from 70% down, 30% up, to 44% down, 56% up – or basically from export to near neutral. The change in the Stones Bay transport is from 75% down, 25% up, to 54% down, 46% up – or again from export to near neutral. We expect that reality lies closer to the uniform particle size distribution than the linear distribution of particle size with depth, particularly during significant resuspension events when the water column is well mixed, and therefore that both bays are net exporters of sediment.

As discussed by Meade (1969), an estuary in equilibrium would have net sediment import in balance with export. During periods of sea level rise sediment accumulates until sediment import again matches sediment export. With a net sediment export, the New River Estuary may be in equilibrium with an excess supply of sediment. However, the period during which we have current measurements and can compute transport is short compared to the multi-decadal time scale of these

effects, consequently the results may be unduly influenced by the increased river flow or spatial variability of sediment import/export. Geyer et al. (2001) shows the Hudson River Estuary net infilling due largely to tidal pumping during a 3 month observation period where net export is expected in the long-term due to excess input from the watershed. Not enough information is available for the New River to establish a definitive long-term trend.

5. Conclusions

An eight-year data set collected by an autonomous profiling buoy at two locations in the New River Estuary provides a unique view of local winds, water column turbidity and sediment resuspension in this mostly wind-driven system. The up estuary site in Morgan Bay has water approximately 3.5 m deep, typical fetch lengths of 1–3 km, weak tidal velocities and is close to the confluence of the New River. The Stones Bay location, approximately 10 km down estuary, was shallower and more exposed, with an average water depth of 2.5 m, fetch lengths of 2–4 km and roughly three times stronger tidal velocities. Winds in Stones Bay are on average 0.5 m s^{-1} stronger than in Morgan Bay.

A subtle (averaging 1 NTU or less over the full data set), but statistically robust turbidity response was identified at diurnal, semi-diurnal and higher frequencies in Stones Bay and to a much lesser extent in Morgan Bay. These were identified with astronomical and shallow water tidal frequencies as well as meteorological phenomena (e.g., the coastal sea breeze). These responses probably represent advection of turbidity gradients past the observation sites. Significant increases in turbidity appeared to be due primarily to resuspension during wind events. Bottom stress due to surface wind waves, as computed from a simple wind-wave model, yielded similar relationships between turbidity and the local wave bottom stress at both measurement locations when all wind directions were combined for turbidity below approximately 17 NTUs, although at highest stresses the turbidity in Stones Bay exceeded that in Morgan Bay. Separating the turbidity response as a function of wind direction showed that significant resuspension events are limited to a small number of directional wind bands (three in Stones Bay and two in Morgan Bay) and that the directional response may be different for each, particularly in Morgan Bay. Assuming the directional response was due to the advection of resuspended material past the measurement site, we identified a consistent relationship between turbidity and bottom stress averaged over the tidal excursion distance in Stones Bay for the three dominant wind forcing directions, providing strong evidence of the resuspension process controlling turbidity over a broad range of forcing at this location. Bottom stress averaged over the upwind direction explained only a part of the directional dependence of the turbidity response in Morgan Bay. During the infrequent, highest wave stress events in Stones Bay and over most of the range of wave stresses in Morgan Bay, it appears that an additional factor is important in determining turbidity levels, presumably sediment characteristics. In particular, winds from the NW in Morgan Bay are directed across the location where the New River enters the much wider New River Estuary. Waves associated with these winds provide the greatest turbidity response, consistent with these sediments being fine, recently deposited and loosely compacted and therefore relatively easy to resuspend compared to sediments in much of the remainder of the estuary.

While multiple previous studies have shown relationships between wave-induced bottom stress and suspended sediment concentrations, having eight years of concurrent data from two locations in the same system allowed us to expose subtleties in these relationships that have not previously been explored. In particular, the directional relationship between turbidity and wave-induced bottom stress suggested the importance of considering the spatial distribution of stress within the system in the analyses. The use of stress averaged over the tidal excursion in areas of significant tidal influence appears robust in this system and stress averaged over the upwind direction in areas of minimal tidal influence also appears to provide some improvement versus local stress calculations for predicting turbidity response.

Resuspension and the resulting suspended sediment concentration are important processes within shallow estuarine systems such as the New River Estuary. Suspended sediment concentrations strongly affect light penetration and photosynthetic processes in the water column and at the sediment surface. Suspension is the primary mechanism for transporting fine sediments through the estuary and the New River Estuary appears to be undergoing a long-term net sediment export. The results presented in this study provide a relatively simple and physics-based methodology for estimating turbidity and, assuming a reasonable calibration between turbidity and sediment concentration, suspended sediment concentrations in the New River Estuary and other similar shallow water estuarine systems.

Acknowledgements

This research was conducted under the Defense Coastal/Estuarine Research Program (DCERP), funded by the Strategic Environmental Research and Development Program (SERDP) Project SI-1413, grant # 1-321-0210294 and 5-312-0213589. Views, opinions, and/or findings contained in this report are those of the author(s) and should not be construed as an official U.S. Department of Defense position or decision unless so designated by other official documentation.

References

Bell, S.B., Sherman, K.M., 1980. A field investigation of meiofaunal dispersal: tidal resuspension and implications. Mar. Ecol. Prog. Ser. 3, 245–249.
Bever, A.J., MacWilliams, M.L., 2013. Simulating sediment transport processes in San Pablo Bay using coupled hydrodynamic, wave, and sediment transport models. Mar. Geol. 345, 235–253.
Bever, A.J., MacWilliams, M.L., Fullerton, D.K., 2018. Influence of an observed decadal decline in wind speed on turbidity in the san Francisco estuary. Estuar. Coast. https://doi.org/10.1007/s12237-018-0403-x.
Booth, J.G., Miller, R.L., McKee, B.A., Leathers, R.A., 2000. Wind-induced bottom sediment resuspension in a micro-tidal coastal environment. Continent. Shelf Res. 20, 785–806.
Carniello, L., D'Alpaos, A., Defina, A., 2011. Modeling wind-waves and tidal flows in shallow microtidal basins. Estuar. Coast Shelf Sci. 92, 263–276. https://doi.org/10.1016/j.ecss.2011.01.001.
Carniello, L., Defina, A., D'Alpaos, L., 2012. Modeling sand-mud transport induced by tidal currents and wind waves in shallow microtidal basins: application to the Venice Lagoon (Italy). Estuar. Coast Shelf Sci. 102–103, 105–115.
Carniello, L., Silvestri, S., Marani, M., D'Alpaos, A., Volpe, V., Defina, A., 2014. Sediment dynamics in shallow tidal basins: in situ observations, satellite retrievals, and numerical modeling in the Venice Lagoon. J. Geophys. Res. Earth Surf. 119, 802–815. https://doi.org/10.1002/2013JF003015.
Carper, G.L., Bachman, R.W., 1984. Wind resuspension of sediments in a prairie lake. Can. J. Fish. Aquat. Sci. 41, 1763–1767.
Clark, T.L., Lesht, B., Young, R.A., Swift, D.J.P., Freeland, G.L., 1982. Sediment Resuspension by surface-wave action: an examination of possible mechanisms. Mar. Geol. 49, 43–59.
Conner, C.S., De Visser, A.M., 1992. A laboratory investigation of particle size effects on an optical backscatterance sensor. Mar. Geol. 108 (2), 151–159.
Dalrymple, R.W., Zailin, B.A., Boyd, R., 1992. Estuarine facies models; conceptual basis and stratigraphic implications. J. Sediment. Res. 62 (6), 1130–1146.
De Jonge, V.N., van Beusekom, J.E.E., 1995. Wind- and tide-induced resuspension of sediment and microphytobenthos from tidal flats in the Ems estuary. Limnol. Oceanogr. 40 (4), 766–778.
Downing, J., 2006. Twenty-five years with OBS sensors: the good, the bad, and the ugly. Continent. Shelf Res. 26 (Issues 17–18), 2299–2318. ISSN 0278-4343. https://doi.org/10.1016/j.csr.2006.07.018.
Dyer, K.R., 1989. Sediment processes in estuaries: future research requirements. J. Geophys. Res. 94 (C10), 14,237–14,339.
Escobar, C.A., Velasquez-Montoya, L., 2017. Modeling the sediment dynamics in the gulf of Urabá, colombian Caribbean sea. Ocean Eng. 147, 476–487. https://doi.org/10.1016/j.oceaneng.2017.10.055.
Fanning, K.A., Carder, K.L., Betzer, P.R., 1981. Sediment resuspension by coastal waters: a potential mechanism for nutrient re-cycling on the ocean's margins. Deep Sea Res. 29 (8A), 953–965.
Fisher, T.R., Carlson, P.R., Barber, R.T., 1982. Sediment nutrient regeneration in three North Carolina estuaries. Estuar. Coast Shelf Sci. 14, 101–116.
Fries, J.S., Characklis, G.W., Noble, R.T., 2006. Attachment of fecal indicator bacteria to particles in the Neuse River Estuary. J. Environ. Eng. 132 (10), 1338–1345.
Geyer, W.R., Woodruff, J.D., andTraykovski, P., 2001. Sediment transport and trapping in the Hudson River estuary. Estuaries 24 (5), 670–679.

Hall, N.S., Paerl, H.W., Peierls, B.L., Whipple, A.C., Rossignol, K.L., 2013. Effects of climatic variability on phytoplankton community structure and bloom development in the eutrophic, microtidal, New River Estuary, North Carolina, USA. Estuar. Coast Shelf Sci. 117 (20), 70–82. https://doi.org/10.1016/j.ecss.2012.10.004.

Hamblin, P.F., 1989. Observations and model of sediment transport near the turbidity maximum of the upper Saint Lawrence Estuary. J. Geophys. Res. 94 (C10), 14,419–14,428. https://doi.org/10.1029/JC094iC10p14419.

Hamilton, D.P., Mitchell, S.F., 1996. An empirical model for sediment resuspension in shallow lakes. Hydrobiologia 317, 209–220.

Ji, Z.G., Jin, K.R., 2014. Impacts of wind waves on sediment transport in a large, shallow lake. Lakes Reservoirs Res. Manag. 19, 118–129.

Lavelle, J.W., Young, R.A., Swift, D.J.P., Clarke, T.L., 1978. Near-bottom sediment concentration and Fluid velocity measurements on the inner continental shelf, New York. J. Geophys. Res. 83 (C12), 6052–6062. https://doi.org/10.1029/JC083iC12p06052.

Lee, C., Schwab, D.J., Beletsky, D., Stroud, J., Lesht, B., 2007. Numerical modeling of mixed sediment resuspension, transport, and deposition during the March 1998 episodic events in southern Lake Michigan. J. Geophys. Res. 112, C02018. https://doi.org/10.1029/2005JC003419.

Lesht, R.A., Clark, T.L., Freeland, G.L., Swift, D.J.P., Young, R.A., 1980. An empirical relationship between the concentration of resuspended sediment and near-bottom orbital velocity. Geophys. Res. Lett. 2, 1049–1052.

Liu, X., Huang, W., 2009. Modeling sediment resuspension and transport induced by storm wind in Apalachicola Bay, USA. Environ. Model. Software 24, 1302–1313.

Luettich Jr., R.A., Harleman, D.R.F., 1990. A Comparison between measured wave properties and simple wave hindcasting models in shallow water. J. Hydraul. Res. 28 (3), 299–308.

Luettich, R.A., Harleman, D.R.F., Somlyódy, L., 1990. Dynamic behavior of suspended sediment concentrations in a shallow lake perturbed by episodic wind events. Limnol. Oceanogr. 35 (5), 1050–1067.

Malhotra, A., Fonseca, M.S., 2007. WEMo (Wave Exposure Model): Formulation, Procedures and Validation. NOAA Technical Memorandum NOS NCCOS #65, Beaufort, North Carolina. pp. 28.

Meade, R.H., 1969. Landward transport of bottom sediments in estuaries of the Atlantic coastal plain. J. Sediment. Petrol. 39 (1), 222–234.

Nakagawa, Y., Sanford, L.P., Halka, J.P., 2000. Effect of wind waves on distribution of muddy bottom sediments in Baltimore Harbor, USA. Coast Eng. 2000, 3516–3524.

Reynolds-Fleming, J.V., Fleming, J.G., Luettich, R.A., 2002. Portable, autonomous vertical profiler for estuarine applications. Estuaries 25 (1), 142–147.

Sanford, L.P., Panageaotu, W., Halka, J.P., 1991. Tidal resuspension of sediments in northern Chesapeake Bay. Mar. Geol. 97 (1–2), 87–103.

Sanford, L.P., 1994. Wave-forced resuspension of upper Chesapeake Bay muds. Estuar. Coast 17 (1), 148–165.

Schallenberg, M., Burns, C.W., 2004. Effects of sediment resuspension on phytoplankton production: teasing apart the influences of light, nutrients and algal entrainment. Freshw. Biol. 49, 143–159. https://doi.org/10.1046/j.1365-2426.2003.01172.x.

Schoellhamer, D.H., 1995. Sediment resuspension mechanisms in old Tampa bay, Florida. Estuar. Coast Shelf Sci. 40, 603–620.

Seers, B.M., Shears, N.T., 2015. Spatio-temporal patterns in coastal turbidity – long-term trends and drivers of variation across an estuarine-open coast gradient. Estuar. Coast Shelf Sci. 154, 137–151. https://doi.org/10.1016/j.ecss.2014.12.018.

U.S. Coastal Engineering Research Center (USCOE), 1977. In: Shore Protection Manual 1 U.S. Army Coastal Engineering Research Center, Ft, Belvoir, Virginia.

Wang, L., Zhou, Y., Shen, F., 2018. Suspended sediment diffusion mechanisms in the Yangtze Estuary influenced by wind fields. Estuar. Coast Shelf Sci. 200, 428–436. https://doi.org/10.1016/j.ecss.2017.11.038.

Ward, L.G., Kemp, W.M., Boynton, W.R., 1984. The influence of waves and seagrass communities on suspended particulates in an estuarine embayment. Mar. Geol. 59 (1–4), 85–103.